The Influence of Mechanical Stresses on the Diffusion and Accumulation of Hydrogen in a Cylindrical Roller Thrust Bearing

Iyas Khader[1,2], Dominik Kürten[2], Andreas Kailer[2]

[1] *Department of Industrial Engineering, German Jordanian University, P.O. Box 35247, 11180 Amman, Jordan,* iyas.khader@gju.edu.jo

[2] *Fraunhofer Institute for Mechanics of Materials IWM, Wöhlerstraße 11, 79108 Freiburg, Germany,* dominik.kuerten@iwm.fraunhofer.de, andreas.kailer@iwm.fraunhofer.de

Abstract– Steel rolling elements in bearings are known to undergo premature failure due to brittle flaking or what is also known as white structure flaking. This failure mode is associated with the formation of white etching cracks (WEC) and white etching areas (WEA). Literature findings point out to the mechanism resulting in early brittle flaking as a form of hydrogen-assisted fatigue; hence, the term hydrogen assisted rolling contact fatigue (HARCF) was coined. Understanding the factors affecting the diffusion and subsurface accumulation of hydrogen in bearing steel is crucial to developing measures to mitigate or completely eliminate its detrimental effect.

In this work, a finite element simulation model of a cylindrical roller thrust bearing (CRTB) was created. The simulations enabled studying the diffusion of hydrogen and obtaining qualitative information pertaining to stress-assisted diffusion in tribological loading under the influence of residual stresses. The simulations revealed rather insignificant hydrogen accumulation due to stress-assisted diffusion in comparison to concentration gradient driven diffusion. On the other hand, residual stresses had an evident influence on the subsurface accumulation of hydrogen. The overlap between regions undergoing high stresses and those showing high concentrations of accumulated hydrogen points out to the triggering mechanism of HARCF.

Keywords – Hydrogen diffusion, residual stresses, roller bearings, hydrogen-assisted rolling contact fatigue, WEA/WEC.

1. Introduction

Premature damage in bearings in the form of brittle flaking is still an open area of research and the causes for its occurrence are discussed quite diversely. There is a plethora of examples in the literature discussing the mechanisms of brittle flaking and despite some contradictions (cf. Harada et al. [1]) there is general consensus that it is a form of hydrogen-assisted fatigue [2, 3, 4, 5, 6]; hence, the term hydrogen assisted rolling contact fatigue (HARCF) was adopted. It was shown in several studies that hydrogen forms in rolling contact due to tribochemical reactions between the lubricant and the steel surface [7, 8, 9, 10, 11, 12] or from additives or contaminants [10, 13, 14, 15] present in the lubricant. The release of hydrogen and formation of hydrocarbon byproducts due to lubricant degradation was confirmed through in-situ measurements using vacuum tribometers [12, 16, 17, 18] and electrochemical cells [19, 20].

HARCF is manifested by inter-crystalline crack growth in the subsurface region of the bearing [17] and brittle flaking (also known as white flaking or white structure flaking), which causes spalling. In many occurrences, HARCF is associated with the presence of white etching cracks (WEC) and microstructural alterations known as white etching areas (WEA), which have been explained in light of crack-face rubbing during over-rolling [21, 22]. Although HARCF has not been confirmed as the only root cause of premature WEC-associated failure, it was observed that the formation of WEC was strongly exacerbated in hydrogen-charged samples once reaching specific concentrations as concluded by the work of several researchers [4, 23, 24, 25, 26]. For instance, Hamada and Matsubara [26] reported premature flaking, the occurrence of distinct microstructural changes and WEC formation in hydrogen pre-charged samples tested in rolling-sliding contact; under identical testing conditions the same effects could not be reproduced at lower hydrogen concentrations. Recently, Liang et al. [27] showed by means of rolling contact fatigue tests on bearing steel that hydrogen facilitates the formation of voids and what the authors described as “typical hydrogen-assisted cracks”; hydrogen pre-charged samples showed higher void and crack length density and longer cracks in comparison to uncharged samples. Ruellan et al. [27] attempted to give an overview of the root causes of early damage associated with WEC formation. In a more recent work, this type of damage was correlated with the lubricant formulation [29] rather than specific additives. Besides HARCF, WEC failures were attributed to adiabatic shearing, corrosion fatigue cracking and inclusions (cf. Stadler et al. [29]). WEC-associated failure is known to occur significantly earlier than predicted by standard bearing lifetime calculations [29]. Statistical data on parts revealing WEC failure showed a steeper failure probability slope than that obtained for bearings undergoing classical rolling contact fatigue (RCF) (typical telltale signs of RCF are discussed in [30]), thus, indicating significantly smaller scatter in lifetime data.

Hydrogen uptake in metals normally takes the form of atomic or ionic hydrogen. A review of hydrogen ingress mechanisms in bearing steel is found in [31]. Within this context, we assume that the most predominant mechanism is due to lubricant degradation and decomposition. Diffusible hydrogen, which may as well be trapped at microstructural defects such as

lattice defects and grain and phase boundaries, is known to induce material degradation in steel in what is known as hydrogen embrittlement [44]. The most prominent theories attempting to explain hydrogen-induced degradation are hydrogen enhanced decohesion (HEDE) and hydrogen-enhanced localized plasticity (HELP) .

Modeling hydrogen diffusion in tribological contact is a challenging task, which may shed light on the causes of premature failure. It was shown in early studies that hydrogen accumulates at regions undergoing tensile stresses such as crack tips [28, 29, 30]. Winzer and Khader [31] modeled hydrogen diffusion and trapping in a twin-disk tribological contact using a weakly-coupled finite element (FE) model. It was shown that stress-assisted diffusion plays a minor role in the accumulation of hydrogen. Kadin [32] simulated the effect of compressive residual stresses on hydrogen diffusion and described their effect in enhancing surface to subsurface transport of hydrogen. In a recent study, Khader et al. [33] showed the effect of residual stresses on the diffusion and subsurface accumulation of hydrogen. It was concluded that certain residual stress profiles may lead to intensified subsurface hydrogen accumulation.

Several researchers have measured residual stress profiles in bearing components [34, 35, 36, 37, 38, 39, 40]. Of particular interest were the X-ray diffraction (XRD) measurements conducted by Voskamp et al. [34], Voskamp and Mittemeijer [38] and Dommarco et al. [35]. Voskamp et al. [34], Voskamp and Mittemeijer [38] reported results on 6309-type deep groove ball bearing inner rings. The tested material was SAE 52100 bearing steel predominantly tempered martensitic with 10-15 vol.% retained austenite and about 3-5 vol.% globular cementite with hardness of 850 HV30. Dommarco et al. [35] conducted the measurements on 9.53 mm diameter rods. The tested material was SAE 52100 bearing steel, martensitic hardened and tempered at various temperatures with hardness values ranging between 58.5 HRC and 62.5 HRC. The published data represented residual stress profiles as function of depth. Prior to testing, the profile in unused through-hardened bearing steel was generally comprised of a compressive stress field on the surface and a tensile stress field in the subsurface (blue curve in *Figure 1*). The residual stresses in [40, 44] were additionally measured following rolling contact fatigue tests carried out at maximum Hertzian contact stresses of 3.3-3.8 GPa. Over-rolling resulted in changing the initial residual stress profile to a one comprised of two compressive stress fields surrounding a tensile stress field in the near-surface region (maroon curve in *Figure 1*).

The aim of this work is to provide an analysis of diffusible hydrogen accumulation in a cylindrical roller thrust bearing (CRTB) in the absence of trapping. This analysis sheds light on a mechanism directly related to hydrogen assisted rolling contact fatigue (HARCF). Hydrogen transport was modeled through two distinct

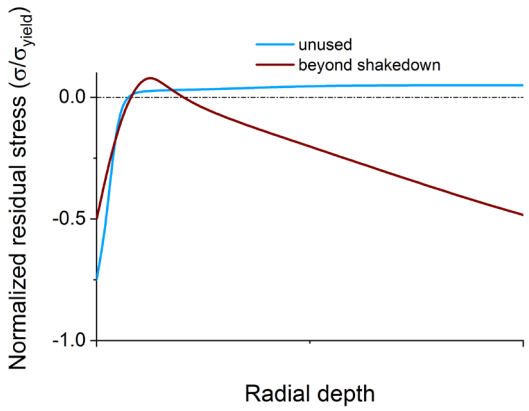

Figure 1: Residual stress profile on the surface and in the subsurface of through hardened bearing steel [34, 38, 35].

mechanisms: (i) concentration gradient driven diffusion and (ii) stress-assisted diffusion. The focus here will be on the influence of various residual stress profiles on the accumulation of subsurface hydrogen.

2. Finite element modeling

A finite element (FE) simulation model was created in Abaqus® to study the diffusion of hydrogen under the influence of various residual stress fields. The developed simulation model is a weakly-coupled, i.e., sequential mechanical-diffusion, two-dimensional extension of the fully-coupled three-dimensional model developed in a previous work [33]. In this work, a structural mechanics simulation was carried out to obtain residual stress profiles, the results of which were then imported into a diffusion simulation. This procedure enables obtaining concentration profiles as function of internal stresses. Notwithstanding the geometrical limitations imposed by modeling the system in two dimensions, this simplification allows for a better understanding of the influence of contact loading on residual stresses and how the latter affects hydrogen diffusion in bearings. Thanks to the manageable model size, two dimensional modeling allows conducting parametric studies. The verification of the Abaqus mass transfer internal code may be consulted in [45].

2.1. Mesh and boundary conditions

A two dimensional section of a cylindrical roller thrust bearing (CRTB) with the dimensions of the commercial bearing FAG 81104-TV was modelled in Abaqus® as shown in *Figure 2*. The average element dimensions in the contact zone were 30 µm×10 µm. The geometry comprised of a section of a roller (diameter Ø = 4.5 mm and length L = 4.5 mm) and the upper and lower raceways. To discretize the geometry, second-order eight-node plane-stress quadrilateral elements (CPS8) were used. A fine mesh was created in the vicinity of the contact zone while discretizing the rest of the geometry with a coarser mesh thus, keeping the size of the model rather manageable.

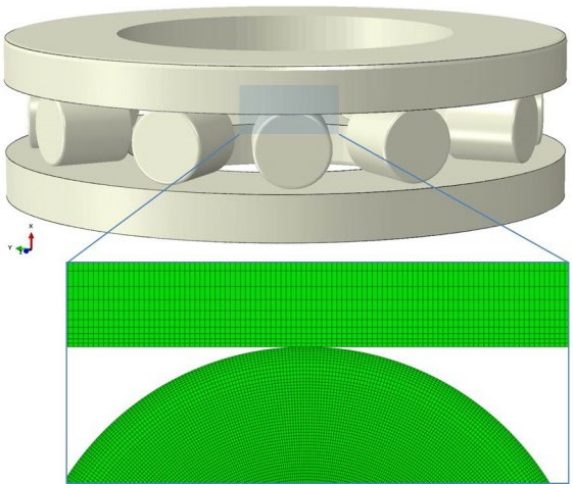

Figure 2: Two-dimensional section of the bearing FAG 81104-TV showing the FE-mesh.

A normal load of 180 N/mm was applied to the upper ring; thus, assuming a line contact, results in a maximum Hertzian contact pressure of 1.7 GPa. Both the upper and lower rings were fixed and the roller was rotated about its axis at an angular velocity of 62.8 rad/s. Coulomb friction was adopted to model friction between the roller and the raceways; the coefficient of friction was assumed constant with a value of $\mu = 0.05$. This value was obtained from a series of measurements carried out on a thrust-bearing tribometer using the same type of bearings and lubricated with a commercial fully-additivated transmission oil with kinematic viscosities of $KV_{40\,°C} = 64.0$ mm^2/s and $KV_{100\,°C} = 9.5$ mm^2/s [33]. It should be pointed out that the friction coefficient measured in full bearing tests has many sources other than solid-to-solid contact (e.g., lubricant viscosity) and hence, does not follow the definition of the friction coefficient according to Coulomb.

For the simulation of diffusion second-order eight-node mass diffusion elements (DC2D8) were used. The stresses were imported from the structural mechanics simulation as initial conditions. Since no knowledge pertaining to either hydrogen flux or hydrogen surface concentration is available, diffusion was assumed to occur uniformly across the roller surface by defining a flux of $J = 10^{-7}$ ppm·mm^2/s. The value was chosen based on a sensitivity analysis carried out to ensure no hydrogen is accumulated in the center of the roller, since hydrogen diffusion from steel into the atmosphere remains unknown. The diffusion period was set to 18×10^3 s. By setting this constraint, diffusion was achieved without having to fix the concentration of surface nodes.

2.2. Residual stresses

The residual stress profiles in the roller were implemented in a preliminary simulation step by applying predefined temperature fields at specific nodes. These boundary conditions were released towards the end of the step to obtain a uniform temperature distribution of 25° C throughout the material and a residual-stress profile in an equilibrium state.

Three residual stress distribution profiles were tested in the simulations as shown in *Figure 3* and detailed as follows:

I. Residual stress free material, exemplified by the black long-dashed curve in *Figure 3*

II. Through-hardened bearing material in its virgin state. Surface machining and heat treatment, resulting in temperature gradients, induce compressive residual stresses on the surface and tensile residual stresses in the subsurface; this profile is denoted by compression-tension (CT) and represented by the blue solid curve in *Figure 3*

III. Bearing steel beyond the shakedown phase with accumulated subsurface plastic strain due to over-rolling. The material lies under two compressive stress fields (on the surface and further down in the subsurface region) surrounding a weaker tensile stress field in the near-surface region. This profile is denoted by compression-tension-compression (CTC) and represented by the green dotted curve in *Figure 3*

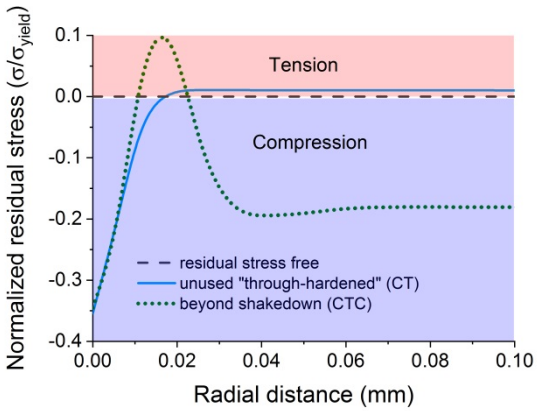

Figure 3: Residual stress distribution profiles implemented in the FE model.

2.3. Diffusion equations

The governing equations for mass diffusion are an extension of Fick's second law. The model accounts for two diffusion mechanisms, namely, (i) diffusion due to the presence of concentration gradients of the diffusing species in the base material and (ii) diffusion driven by stress gradients. The diffusion equation obeys the principles of mass conservation given in the form

$$\frac{\partial}{\partial t}\int_V \bar{C}\,dV + \int_{\partial V} \boldsymbol{n}\cdot\boldsymbol{J}\,dS = 0 \qquad \text{(Eq. 1)}$$

where t is the diffusion time, V is any volume whose surface is S, $\mathbf{n}$ is the outward normal to S, $\bar{C}$ is the total molar concentration of hydrogen and $\boldsymbol{J}$ is the flux.

Assuming a constant temperature, the constitutive expression of the flux is given by [28]

$$\boldsymbol{J} = \frac{D_L \bar{V}_H \bar{C}}{RT}\nabla\sigma_h - D_L\nabla\bar{C} \qquad \text{(Eq. 2)}$$

where D_L is the lattice diffusivity of hydrogen, $\bar{V}_H$ is the partial molar volume of hydrogen dissolved in the host material, σ_h is the hydrostatic stress given by ($\sigma_h = -trace(\boldsymbol{\sigma})/3$), R is the ideal gas constant, T is the absolute temperature in kelvin and $\nabla\sigma_h$ and $\nabla\bar{C}$ are the spatial gradients of the hydrostatic pressure and molar concentration, respectively. Within this context, the form presented in *Eq. 2* assumes a negligible concentration of trapped hydrogen in the base material; this assumption was verified for hardened steel 100Cr6 in Kürten et al. [41] by calculating the ratio of trapped to released hydrogen.

2.4. Material constants and simulation parameters

Elastic-plastic material behavior with kinematic strain-hardening was used to model bearing steel (100Cr6). An elastic modulus of E = 200.2 GPa [33] and a Poisson's ratio of ν = 0.3 [42] were used to define the elastic response. Plasticity was incorporated by assuming an initial yield strength of σ_0 = 750 MPa [43] and a linear kinematic strain hardening modulus of H = 185.5 GPa [33], which should give good approximation with measured values up to a plastic strain of ϵ^{pl} = 0.005.

The parameters used in implementing the hydrogen diffusion model are listed in *Table 1*.

Table 1. Material data required for the diffusion model

Property	Unit	Value	Source
Lattice diffusivity (D_L)	mm²/s	1.1×10^{-3}	[44, 45, 46]
Initial hydrogen concentration (C_0)	ppm	1.5	-
Hydrogen flux (J)	ppm·mm²/s	10^{-7}	-
Ideal gas constant (R)	mJ/mol·K	8.314×10^{3}	-
Temperature (T)	K	293.15	-
Partial molar volume (pmv) of dissolved hydrogen in pure iron [unstrained lattice] ($\bar{V}_H$)	mm³/mol	2.0×10^{3}	[47, 48, 49]
Lower and upper values for $\bar{V}_H$	mm³/mol	2.0×10^{3}, 4.0×10^{3}	-

An arbitrary initial hydrogen concentration in steel was set to 1.5 ppm. This value is considered somewhat high as hydrogen concentration in commercial bearing steel may be as low as 0.4 ppm [56] and typically about 1.0 ppm [8, 22]. As shown in *Table 1*, the partial molar volume (pmv) of dissolved hydrogen in steel ($\bar{V}_H$) is given for the unstrained lattice of the host metal. Unlike the diffusion coefficient which is independent of the stress state, the pmv is sensitive to local stress fields [50] and thus, lattice expansion due to elastic stress fields may result in accommodating more hydrogen into the metal [46]. The pmv of hydrogen in iron is about $\bar{V}_H = 2.0\times10^{3}$ mm³/mol for the unstrained lattice; however, depending on the vacancy concentration in the host material, values as high as $\bar{V}_H = 16.3\times10^{3}$ mm³/mol [46] were reported in the literature for the elastically distorted lattice. Moreover, depending on the type of alloy under consideration the pmv may attain different values, for instance Guedes et al. [51] reported values much higher than that in pure iron for martensitic steel alloys. Hence, in this work, and for comparison purposes, a lower value of $\bar{V}_H = 2.0\times10^{3}$ mm³/mol and an upper value of $\bar{V}_H = 4.0\times10^{3}$ mm³/mol will be adopted in the simulations.

3. Results

3.1. Mechanical solution

To simulate the evolution of residual stresses with over-rolling, a simulation was created with a residual stress profile CT, as reported in the literature, and exemplified by the blue solid curve in *Figure 3*. This stress profile resembles that of an unused through-hardened bearing. By applying a load of 180 N/mm, the initial contact stress was 1.63 GPa and the maximum von Mises stress appeared approx. 40 µm below the surface with a peak value of 925 MPa; *Figure 4*.

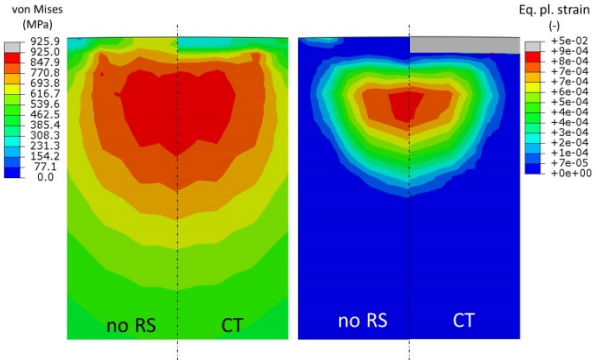

Figure 4: von Mises stress and equivalent plastic strain distributions in the depth of the roller for residual stress free material (no RS) and residual stress profile CT.

To compare this case with a residual stress free material (no RS), the latter was simulated and the results were as follows: The maximum contact stress was 1.73 GPa, which is within 5% of the value obtained from a Hertzian contact solution, and the von Mises stress showed identical values and location to the case with a CT stress profile. Since the developed stresses in the subsurface exceed the initial yield strength of the material (σ_0 = 750 MPa), it is expected that subsurface plastic strain will build up and accumulate.

The initial contact cycle gave rise to fully-contained (i.e., plastically deformed material surrounded by material undergoing only elastic strains) equivalent plastic strain with a maximum value of $\epsilon^{pl} = 9\times10^{-4}$ (refer to *Figure 4*).

During the running-in phase, the bearing material will undergo shakedown, during which subsurface plastic

strain will be accumulated and may even reach the surface in the form of microplasticity. It is hence, expected that residual stresses change from compression on the surface and tension in the subsurface (i.e., compression-tension: CT, exemplified by the blue solid curve in *Figure 3*) to compression on the surface, tension in the immediate subsurface and compression further below in the subsurface (i.e., compression-tension-compression: CTC) as reported in the literature [34, 38, 35] and exemplified by the green dotted curve in *Figure 3*. To examine this proposition, a structural-mechanics simulation with an initial compression-tension (CT) residual stress profile was run for durations of 50 and 100 stress cycles, respectively. The resulting residual stress were plotted against the radial distance in the roller and compared to the initial stress profile as shown in *Figure 5*.

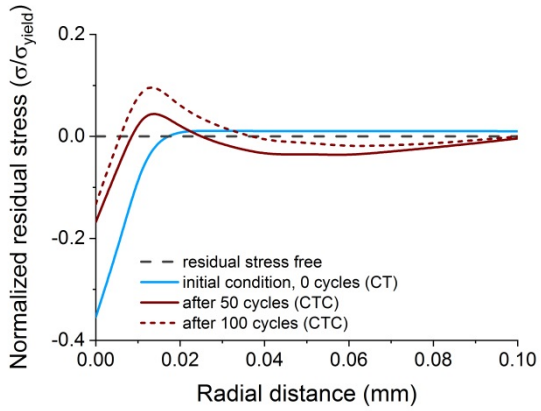

Figure 5: Residual stress profiles obtained from the simulations.

The simulation shows that after 50 stress cycles the residual stress profile changes from CT (blue solid curve in *Figure 5*) to CTC (maroon solid curve in *Figure 5*) and showing reduced compression on the surface. After 100 stress cycles, the compression on the surface slightly decreases and the tensile stress increases resulting in a CTC profile with a steeper gradient (maroon dashed curve in *Figure 5*).

The residual stress profiles obtained from the structural mechanics simulation were then imported as predefined fields into the hydrogen diffusion model. The simulations of hydrogen diffusion into the roller were thus carried out for the four cases of residual stress profiles depicted in *Figure 5*, i.e., (i) residual stress free, (ii) CT as in an unused bearing, (iii) CTC after 50 stress cycles and (iv) CTC after stress 100 cycles.

3.2. Hydrogen diffusion

The results of the diffusion simulations were obtained as nodal concentration values. These were then normalized to the initial hydrogen concentration in the roller (C_0) and plotted against the radial depth in the roller.

3.2.1. The effect of residual stress distribution

In *Figure 6* the hydrogen concentration profiles in the depth of the roller were obtained for the four predefined residual stress profiles shown in *Figure 5*.

In a residual stress free material (black long-dashed curves in *Figure 5* and *Figure 6*), the hydrogen concentration shows a decrease by increasing radial depth. For the case CT (blue solid curves in *Figure 5* and *Figure 6*), which resembles an unused through-hardened bearing, the hydrogen is repelled from the surface into the subsurface and thus, shows slightly higher concentration below the surface.

After 50 stress cycles (maroon solid curves in *Figure 5* and *Figure 6*), the simulation indicates an increased subsurface accumulation of hydrogen, which is exacerbated after 100 cycles (maroon dashed curves in *Figure 5* and *Figure 6*) reaching a value of almost 2.5 times its original concentration in the material at a depth of approx. 12 µm below the surface.

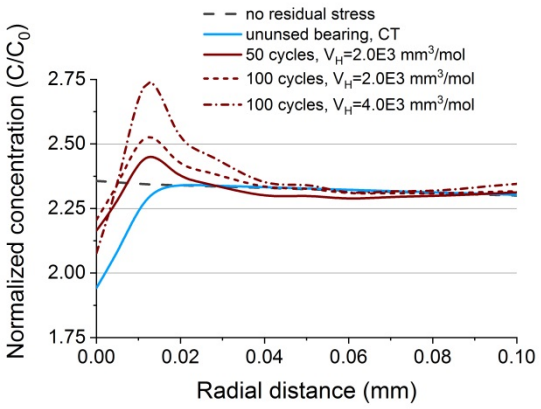

Figure 6: Hydrogen concentration profiles in the depth of the roller.

3.2.2. The effect of the pmv of hydrogen in steel

To study the effect of the pmv of hydrogen in steel, its value was increased to $\bar{V}_H = 4.0\times10^3$ mm^3/mol, which may occur due to elastic stress fields. The hydrogen concentration profile for this case (maroon dot-dash curve in *Figure 6*) showed the value of subsurface accumulated hydrogen to have increased to 2.75 times its original concentration after 100 stress cycles.

3.2.3. The effect of the stress gradient

By going back to *Eq.* 2, it is shown that in fact it is the stress gradient rather than the stress magnitude that provides the driving force for stress-assisted diffusion. To investigate the influence of the stress gradient on the accumulation of hydrogen, the diffusion simulation was carried out with an initial residual stress profile of compression-tension-compression (CTC) as the one depicted in *Figure 3*. As opposed to the CTC-type stress gradients obtained after 50 and 100 stress cycles, this stress profile is characterized by a steep gradient between its compressive and tensile components; such residual stress profile is expected to develop in the bearing well beyond the shakedown phase as reported in the literature.

The results of this simulation is plotted in *Figure* 7 and compared to the results of the simulation results. For this steep stress profile, the subsurface hydrogen accumulation exceeds 3.25 times its original concentration in the material.

For the sake of comparison, the normalized von Mises stress profiles in the unused state (0 cycles, CT) and after 100 stress cycles are plotted against the radial distance in the depth of the roller in *Figure* 7. The von Mises stress profile shows two distinct features regarding its peak between zero and 100 stress cycles: (i) it shifts its position towards the surface of the material and (ii) it increases its value by approx. 20%.

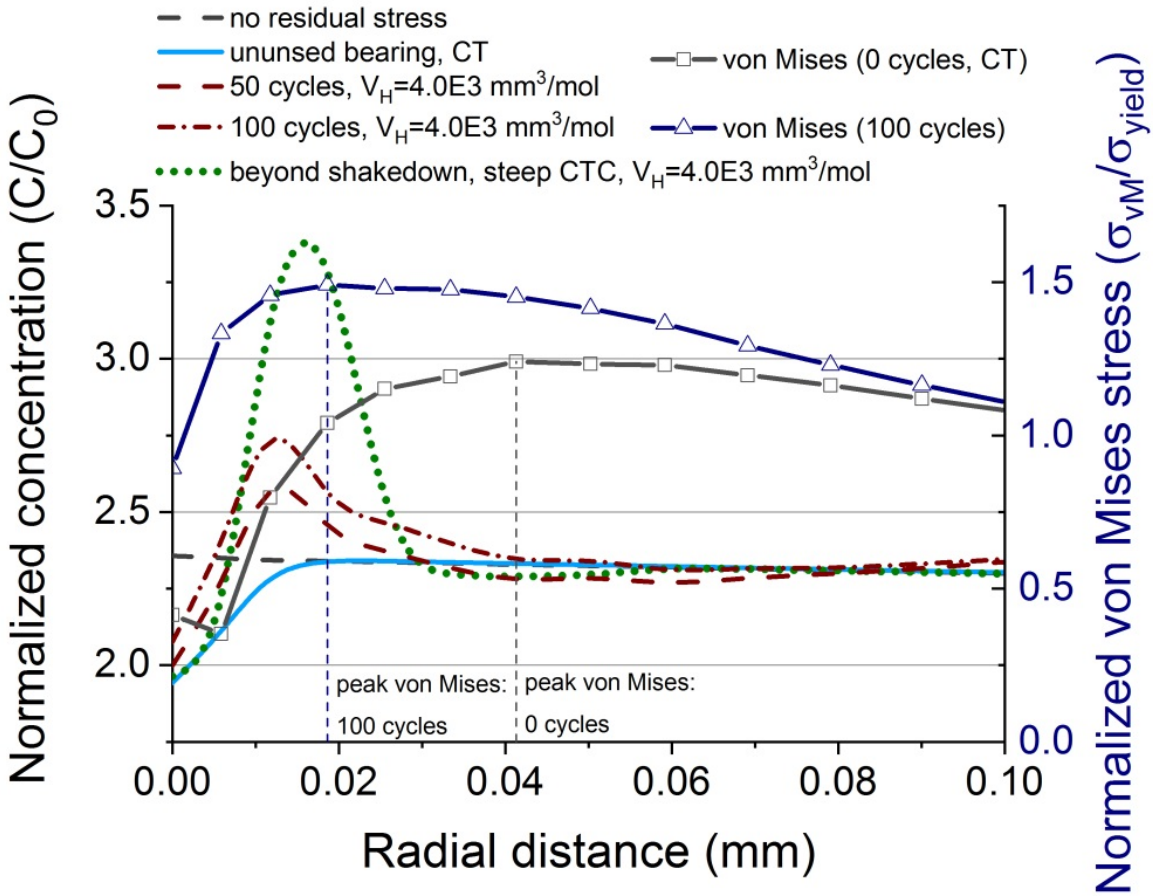

Figure 7: Normalized hydrogen concentration and von Mises stress profiles in the depth of the roller.

4. Discussion

The slight difference in contact stress (below 5%) between the simulation model and the Hertzian contact solution is attributed to: (i) the incorporation of friction and (ii) plasticity in the FE-model, whereas the Hertzian contact model by definition assumes a frictionless elastic contact.

During over-rolling and the associated shakedown of the bearing steel, plastic deformation accumulates below the surface causing the residual stress distribution profile to change from compressive stress on the surface and tensile stress in the subsurface (compression-tension, CT) into two compression stress fields on the surface and in the subsurface surrounding a tensile stress field in the near-surface region (compression-tension-compression, CTC). The results obtained thus far (*Figure 5*) confirm the literature findings [34, 38, 35] that describe such an alteration in residual stresses.

The presence of compressive residual stresses on the surface contributes to the accumulation of subsurface hydrogen. This is in line with the findings of Kadin [32], in which the researcher demonstrated that compressive surface residual stresses enhance surface to subsurface transport of hydrogen. The results of the current study indicate that the presence of residual stresses in the unused bearing may not only drive hydrogen transport but also intensify its subsurface accumulation due to the evolving stress state as a consequence of over-rolling.

The presence of surface compressive residual stresses caused a decrease in hydrogen concertation on the surface compared to the residual-stress-free state (compare "unused bearing, CT" with "no residual stress" in *Figure 6*). After 50 stress cycles, a zone of tensile stress surrounded by an upper and lower zones of compressive stresses is developed due to over-rolling and accumulation of subsurface plastic strain (refer to *Figure 5*). The presence of a tensile stress region surrounded by two compressive stress regions created a preferential path for the subsurface transport of hydrogen causing its repellence from the compressive zones and accumulation in the tensile zone; (compare "50 cycles" with "unused bearing, CT" in *Figure 6*).

Given the uncertainty regarding the partial molar volume of dissolved hydrogen in steel (pmv), lower and upper values for $\bar{V}_H$ of 2.0×10^3 mm^3/mol and 4.0×10^3 mm^3/mol were evaluated. By considering the flux equation (*Eq. 2*) it is apparent that increasing the pmv results in more prominent stress-assisted diffusion leading to more sensitivity to stress gradients. This effect is shown when comparing the results of the 100-cycle simulations carried out with different $\bar{V}_H$ values (*Figure 6*).

Despite the limitation of the current model, especially its crude treatment of boundary conditions pertaining to hydrogen ingress, it clarifies the mechanism of hydrogen accumulation in regions known to undergo fatigue damage due to subsurface stresses. It should be noted that the influence of traps (e.g., dislocations and vacancies) on hydrogen trapping was deliberately not taken into consideration in this model. By disregarding the effect of trapped hydrogen, it was shown here that the accumulation of subsurface hydrogen is essentially independent of trapping. Nevertheless, it should be noted that deformation-induced traps may have an influence on the total hydrogen concentration in the material as demonstrated in previous studies [31, 33] as elevated concentrations of trapped hydrogen are expected to appear within the plastic zone.

In light of these results it may be concluded that a threshold hydrogen concentration for a ductile-to-brittle-transition may be required to trigger crack formation and premature bearing failure. Such a value was reported in the literature to be as low as 1.5 ppm [52] in α-Fe. To put these results in a bigger picture, a critical combination of mechanical stress (in the vicinity of the peak von Mises stresses) and a certain degree of material degradation/embrittlement is required to prompt premature damage. The subsurface distribution of von Mises stresses is thus, shown in *Figure* 7.

In its initial state (0 cycles) the stress profile matches the typical distribution arising in rolling contact with low friction forces. With the progressive accumulation of plastic strain and its consequent strain hardening, the peak von Mises stress shifts its position towards the surface (compare 0 cycles with 100 cycles in *Figure* 7) an thus, approaches the zone of highest hydrogen accumulation in the material; this overlap may contribute to the acceleration of fatigue processes. It was reported by Spriestersbach and Kerscher [53] that microstructural changes in bearing steel, described by the authors as fine granular area (FGA), may be directly correlated with the local plasticity zone predicted by the von Mises criterion, hence, pointing out to the mechanism of formation of FGA. This corroborates the findings of a more recent study [8], which confirmed that telltale features of HARCF such as WEC, from which brittle flaking initiates, appear predominantly in the vicinity of the peak von Mises stresses. It should be however noted that tracing the locations of early signs of damage, such as initiation sites of WEC, is difficult to accomplish experimentally due to the inability to accurately estimate of the minimum number of stress cycles until the first signs of damage appear; the location is also very challenging to predict by numerical simulations due to the sudden changes occurring to the stress state once discontinuities, caused by crack formation, are present in the material.

It was shown in this work that residual stresses induced by machining and hardening processes have a substantial effect on the subsurface accumulation of

hydrogen in bearing steel. Tensile residual stresses such as those present at crack tips or at the tips of inclusions (cf. Al-Tameemi and Long [53]) may also contribute to elevated concentrations of accumulated diffusible hydrogen. In a study conducted by Errichello et al. [55], it was reported that through-hardened bearings fail by cracks that propagate radially and display WEA as sign of microstructural alterations, whereas, carburized steel bearings, that have higher amount of retained austenite and whose residual stress profile is entirely compressive, show higher fracture resistance and tend to fail by macropitting. Nevertheless, reported cases of case-carburized bearings failing due to WEC are present in the literature [64, 65].

The results presented in this study validate those obtained in a previous study [33], in which residual stress profiles were solely based on literature data. The applicability of the developed model to lifetime assessment of real bearings would be greatly improved by considering more realistic boundary conditions pertaining to hydrogen ingress in addition to credible measurements of residual stresses.

5. Conclusions

In this work a weakly-coupled mechanical-diffusion simulation was conducted to study the influence of mechanical stresses on the diffusion and accumulation of hydrogen in a bearing contact. The following is concluded:

- The simulations highlighted that over-rolling and accumulation of subsurface plastic strain, during bearing operation, lead to an alteration of residual stresses. A residual stress profile of compression on the surface and tension in the subsurface will change to compression-tension-compression due to rolling contact.
- Subsurface plastic deformation caused by rolling contact causes the peak von Mises stress to change its value and shift its position towards the surface of the bearing component.
- The presence of residual stresses with a positive gradient (compression to tension) promotes the subsurface transport of hydrogen and its accumulation in the tensile stress region.
- The overlap of high subsurface hydrogen concentration (promoted by residual stresses) and high mechanical stresses (in the vicinity of the peak of von Mises stress) sheds light on the mechanism of hydrogen assisted rolling contact fatigue (HARCF) in bearing steel.

6. References

[1] H. Harada, T. Mikami, M. Shibata, D. Sokai, A. Yamamoto and H. Tsubakino, "Microstructural changes and crack initiation with white etching area formation under rolling/sliding contact in bearing steel," *ISIJ International,* vol. 45, no. 12, pp. 1897-1902, 2005.

[2] K. Tamada and H. Tanaka, "Occurrence of brittle flaking on bearings used for automotive electrical instruments and auxiliary devices," *Wear,* vol. 199, pp. 245-252, 1996.

[3] M.-H. Evans, A. Richardson, L. Wang and R. Wood, "Effect of hydrogen on butterfly and white etching crack (WEC) formation under rolling contact fatigue (RCF)," Wear, vol. 306, no. 1-2, pp. 226-241, 2013.

[4] N. Kino and K. Otani, "The influence of hydrogen on rolling contact fatigue life and its improvement," *JSAE Review,* vol. 24, no. 3, pp. 289-294, 2003.

[5] T. Endo, D. Dong, Y. Imai and Y. Yamamoto, "Study on Rolling Contact Fatigue in Hydrogen Atmosphere - Improvement of Rolling Contact Fatigue Life by Formation of Surface Film," in *Tribology and Interface Engineering Series*, vol. 48, D. Dowson, M. Priest, G. Dalmaz and A. Lubrecht, Eds., Elsevier, 2005, pp. 343-350.

[6] Y. Imai, T. Endo, D. Dong and Y. Yamamoto, "Study on rolling contact fatigue in hydrogen environment at a contact pressure below basic static load capacity," *Tribology Transactions,* vol. 53, pp. 764-770, 2010.

[7] D. Kuerten, N. Winzer, A. Kailer, W. Pfeifer, R. Spallek and M. Scherge, "In-situ detection of hydrogen evolution in a lubricated sliding pin on disk test under high vacuum," *Tribology International,* pp. 324-331, 2016.

[8] D. Kürten, I. Khader, R. Raga, P. Casajús, N. Winzer, R. Spallek, M. Scherge and A. Kailer, "Hydrogen assisted rolling contact fatigue due to lubricant degradation and formation of white etching areas," *Engineering Failure Analysis,* vol. 99, pp. 330-342, 2019.

[9] M. Ratoi, H. Tanaka, B. Mellor and J. Sugimura, "Hydrocarbon lubricants can control hydrogen embrittlement," *Scientific Reports,* vol. 10, p. 1361, 2020.

[10] B. Han, J. Binns and I. Nedelcu, "In situ detection of hydrogen uptake from lubricated rubbing contacts," *Tribology Online,* vol. 2, pp. 450-454, 2016.

[11] M. Kohara, T. Kawamura and M. Egami, "Study on mechanism of hydrogen generation from lubricants," *Tribology Transactions,* vol. 49, pp. 53-60, 2006.

[12] R. Lu, I. Minami, H. Nanao and S. Mori, "Investigation of decomposition of

hydrocarbon oil on the nascent surface of steel," *Tribology Letters,* vol. 27, no. 1, pp. 25-30, 2007.

[13] R. Lu, S. Mori, T. Kubo and H. Nanao, "Effect of sulfur-containing additive on the decomposition of multialkylated cyclopentane oil on the nascent steel surface," *Wear,* vol. 267, pp. 1430-1435, 2009.

[14] R. Lu, S. Mori, H. Nanao, K. Kobayashi and I. Minami, "Study on decomposition of multialkylated cyclopentane oil with sulfur-containing additive on the nascent steel surface," *Tribology Online,* vol. 2, pp. 105-109, 2007.

[15] E. Esfahani, S. Soltanahmadi, A. Morina, B. Han, I. Nedelcu, M. C. van Eijk and A. Neville, "The multiple roles of a chemical tribofilm in hydrogen uptake from lubricated rubbing contacts," *Tribology International,* p. 106023, 2019.

[16] P. A. Bertrand, "Low-Energy-Electron-Stimulated Degradation of a Multiply Alkylated Cyclopentane Oil and Implications for Space Bearings," *Tribology Letters,* 2010.

[17] D. Kuerten, Einfluss der tribochemischen Schmierstoffoxidation auf die wasserstoffinduzierte Wälzkontaktermüdung, PhD Thesis, Fraunhofer Verlag, 2015.

[18] D. Kürten, I. Khader and A. Kailer, "Tribochemical degradation of vacuum-stable lubricants: A comparative study between multi-alkylated cyclopentane and perfluoropolyether in a vacuum ball-on-disk and full-bearing tests," Lubrication Science, pp. 1-9, 2020.

[19] E. Esfahani, A. Morina, B. Han, I. Nedelcu, M. C. van Eijk and A. Neville, "Development of a novel in-situ technique for hydrogen uptake evaluation from a lubricated tribocontact," *Tribology International,* vol. 113, pp. 433-442, 2017.

[20] N. Oberle, T. Amann, D. Kürten, R. Raga and A. Kailer, "In-situ-determination of tribologically induced hydrogen permeation using electrochemical methods," *Proceedings of the Institution of Mechanical Engineers, Part J: Journal of Engineering Tribology,* 2019.

[21] R. Vegter and J. Slycke, "The role of hydrogen on rolling contact fatigue response of rolling element bearings," *ASTM International,* vol. 7, p. 12, 2010.

[22] H. Bhadeshia, "Steels for bearings," *Progress in Materials Science,* vol. 57, no. 2, pp. 268-435, 2012.

[23] H. Uyama, H. Yamada, H. Hidaka and N. Mitamura, "The effects of hydrogen on microstructural change and surface originated flaking in rolling contact fatigue," *Tribology Online,* vol. 6, no. 2, pp. 123-132, 2011.

[24] M. Oezel, A. Schwedt, T. Janitzky, R. Kelley, C. Bouchet-Marquis, L. Pullan, C. Broeckmann and J. Mayer, "Formation of white etching areas in SAE 52100 bearing steel under rolling contact fatigue – Influence of diffusible hydrogen,," *Wear,* vol. 414–415, pp. 352-365, 2018.

[25] M. Curd, T. Burnett, J. Fellowes, J. Donoghue, P. Yan and P. Withers, "The heterogenous distribution of white etching matter (WEM) around subsurface cracks in bearing steels," *Acta Materialia,* vol. 174, pp. 300-309, 2019.

[26] H. Hamada and Y. Matsubara, "The influence of hydrogen on tension-compression and rolling contact fatigue properties of bearing steel," NTN Technical Review, vol. 74, pp. 54-60, 2006.

[27] X. Liang, G.-H. Zhao, J. Owens, P. Gong, W. Rainforth and P. Rivera-Díaz-del-Castillo, "Hydrogen-assisted microcrack formation in bearing steels under rolling contact fatigue," *International Journal of Fatigue,* vol. 134, p. 105485, 2020.

[28] A. Ruellan, F. Ville, X. Kleber, C. Burnet, D. Girodin and J. Cavoret, "Understanding white etching cracks in rolling element bearings: Formation mechanisms and influent tribochemical drivers," *Proceedings of the Institution of Mechanical Engineers, Part J: Journal of Engineering Tribology,* vol. 229, no. 8, pp. 886-901, 2015.

[29] A. Ruellan, K. Stadler, J. Jelita Rydel and H. Ryan, "The influence of lubricant formulation on early thrust and radial bearing damage associated with white etching cracks," Proceedings of the Institution of Mechanical Engineers, Part J: Journal of Engineering Tribology, 2020.

[30] K. Stadler, Lai, J. and R. Vegter, "A review: The dilemma with premature white etching crack (WEC) bearing failures," in Bearing Steel Technologies: 10th Volume, Advances in Steel Technologies for Rolling Bearings, J. Beswick, Ed., West Conshohocken, PA, 2014, pp. 487-508.

[31] A. Olver, "The mechanism of rolling contact fatigue: An update," *Proceedings of the Institution of Mechanical Engineers, Part J: Journal of Engineering Tribology,* vol. 219, no. 5, pp. 313-330, 2005.

[32] M. A. Stopher and P. Rivera-Diaz-del-Castillo, "Hydrogen embrittlement in bearing steels," *Materials Science and Technology,* vol. 32:11, pp. 1184-1193, 2016.

[33] R. Oriani, "Hydrogen embrittlement of steels," *Annual Review of Materials Science,* vol. 8, pp. 327-357, 1978.

[34] P. Sofronis and R. McMeeking, "Numerical analysis of hydrogen transport near a blunting crack tip," *Journal of the Mechanics and Physics of Solids,* vol. 37, no. 3, pp. 317-350, 1989.

[35] A. Varias and A. Massih, "Hydride-induced embrittlement and fracture in metals - effect of stress and temperature distribution," *Journal of the Mechanics and Physics of Solids,* vol. 50, no. 7, p. 2002, 1469-1510.

[36] A. Krom, R. Koers and A. Bakkar, "Hydrogen transport near a blunting crack tip," *Journal of the Mechanics and Physics of Solids,* vol. 47, no. 4, pp. 971-992, 1999.

[37] N. Winzer and I. Khader, "Hydrogen diffusion and trapping in bodies undergoing rolling contact," *Wear,* vol. 303, no. 1-2, pp. 451-458, 2013.

[38] Y. Kadin, "Modeling of hydrogen transport in static and rolling contact," *Tribology Transactions,* vol. 58, no. 2, pp. 260-273, 2015.

[39] I. Khader, D. Kürten, R. Raga, N. Winzer and A. Kailer, "Modeling hydrogen diffusion in a tribological scenario: A failure analysis of a thrust bearing," *Wear,* Vols. 438-439, p. 203054, 2019.

[40] A. Voskamp, R. Österlund, P. Becker and O. Vingsbo, "Gradual changes in residual stress and microstructure during contact fatigue in ball bearings," *Metals Technology,* vol. 1, no. 7, 1980.

[41] R. Dommarco, K. Kozaczek, P. Bastias, G. Hahn and C. Rubin, "Residual stresses and retained austenite evolution in SAE 52100 steel under non-ideal rolling contact loading," *Wear,* vol. 257, no. 11, pp. 1081-1088, 2004.

[42] V. Güley, A. E. Tekkaya, T. Savaş and F. Özhan, "Experimental investigation of residual stresses after heat treatment and grinding processes in the production of ball bearing rings," *Materials Science Forum,* Vols. 571-572, pp. 27-32, 2008.

[43] C. A. Stickels and A. M. Janotik, "Controlling residual stresses in 52100 bearing steel by heat treatment," *Metallurgical Transactions A,* vol. 11, no. 3, pp. 467-473, 1980.

[44] A. Voskamp and E. Mittemeijer, "State of residual stress induced by cyclic rolling contact loading," *Materials Science and Technology,* vol. 13, no. 5, pp. 430-438, 1997.

[45] B. Gould, M. Paladugu, N. Demas, A. Greco and R. Hyde, "Figure the impact of steel microstructure and heat treatment on the formation of white etching cracks," *Tribology International,* vol. 134, pp. 232-239, 2019.

[46] M. Paladugu and R. Hyde, "Material composition and heat treatment related influences in resisting rolling contact fatigue under WEC damage conditions," *International Journal of Fatigue,* vol. 134, p. 105476, 2020.

[47] D. Systèmes, "SIMULIA User Assistance 2018: Abaqus Verification Guide," Dassault Systèmes Simulia Corp., 2017.

[48] D. Kürten, I. Khader and A. Kailer, "Determining the effective hydrogen diffusion coefficient in 100Cr6," Materials and Corrosion, pp. 1-6, 2020.

[49] C. Acht, M. Dalgic, F. Frerichs, M. Hunkel, A. Irretier, T. Lübben and H. Surm, "Ermittlung der Materialdaten zur Simulation des Durchhärtens von Komponenten aus 100Cr6. Teil 1," *HTM Journal of Heat Treatment and Materials,* vol. 63, no. 5, 2008.

[50] F. Yoshida, "A constitutive model of cyclic plasticity," *International Journal of Plasticity,* vol. 16, no. 3-4, pp. 359-380, 2000.

[51] Y. Efimenko, A. Kuslitskii, D. Chaban, G. Karpenko and B. Movchan, "Effect of electron-beam melting upon the properties of grade ShKhl5 ball-bearing steel," *Fiziko-Khimicheskaya Mekhanika Materialov,* vol. 1, no. 4, pp. 333-335, 1965.

[52] J. Bogkris, W. Beck, M. Genshaw, P. Subramanyan and F. Williams, "The effect of stress on the chemical potential of hydrogen in iron and steel," *Acta Metallurgica,* vol. 19, no. 11, pp. 1209-1218, 1971.

[53] S. Frappart, X. Feaugas, J. Creus, F. Thebault, L. Delattre and H. Marchebois, "Hydrogen solubility, diffusivity and trapping in a tempered Fe–C–Cr martensitic steel under various mechanical stress states," *Materials Science and Engineering: A,* vol. 534, pp. 384-393, 2012.

[54] D. Guedes, A. Oudriss, S. Frappart, G. Courlit, S. Cohendoz, P. Girault, J. Creus, J. Bouhattate, A. Metsue, F. Thebault, L. Delattre, D. Koschel and X. Feaugas, "The influence of hydrostatic stress states on the hydrogen solubility in martensitic steels," *Scripta Materialia,* Vols. 84-85, pp. 23-26, 2014.

[55] J. Choi, "Diffusion of hydrogen in iron," *Metallurgical Transactions,* vol. 1, pp. 911-919, 1970.

[56] H. Hagi, Y. Hayashi and N. Ohtani, "Diffusion coefficient of hydrogen in pure iron between 230 and 300K," *Transactions of the Japan Institute of Metals,* vol. 20, no. 7, pp. 349-357, 1979.

[57] J. Hirth, "Effects of hydrogen on the properties of iron and steel," *Metallurgical Transactions A,* vol. 11A, pp. 861-890, 1980.

[58] L.-C. Hwang and T.-P. Perng, "Hydrogen transport in ferritic stainless steel under elastic

stress," *Materials Chemistry and Physics,* vol. 36, pp. 231-235, 1994.

[59] C. Sturges and A. Miodownik, "The interaction of hydrogen and dislocations in iron," *Acta Metallurgica,* vol. 17, no. 9, pp. 1197-1207, 1969.

[60] J. O. Bockris, W. Beck, M. Genshaw, P. Subramanyan and F. Williams, "The effect of stress on the chemical potential of hydrogen in iron and steel," *Acta Metallurgica,* vol. 19, no. 11, pp. 1209-1218, 1971.

[61] D. K. E. Spriestersbach, "The role of local plasticity during very high cycle fatigue crack initiation in high-strength steels," *International Journal of Fatigue,* vol. 111, pp. 93-100, 2018.

[62] H. Al-Tameemi and H. Long, "Finite element simulation of subsurface initiated damage from non-metallic inclusions in wind turbine gearbox bearings," *International Journal of Fatigue,* vol. 131, p. 105347, 2020.

[63] R. Errichello, R. Budny and R. Eckert, "Investigations of bearing failures associated with white etching areas (WEAs) in wind turbine gearboxes," *Tribology Transactions,* vol. 56, no. 6, pp. 1069-1076, 2013.

[64] K. Stadler and A. Stubenrauch, "Premature bearing failures in wind gearboxes and white etching cracks (WEC)," SKF Evolution, 2013.

[65] R. Budny, "Research on white Etch crack failures and failure prevention," in *AWEA Windpower 2015, May 18-21*, Orlando, 2015.